Enhanced second harmonic generation from coupled asymmetric plasmonic metal nanostructures

Bilge Can Yildiz[1,2,3,4,7]**, Mehmet Emre Tasgin**[4]**, Musa Kurtulus Abak**[2,5]**,
Sahin Coskun**[2,6]**, Husnu Emrah Unalan**[2,5,6] **and Alpan Bek**[1,2,5]

[1] Department of Physics, Middle East Technical University, 06800, Ankara, Turkey
[2] The Center for Solar Energy Research and Applications (GUNAM), Middle East Technical University, 06800, Ankara, Turkey
[3] Physics Unit, Atilim University, 06836 Ankara, Turkey
[4] Institute of Nuclear Sciences, Hacettepe University, 06800, Ankara, Turkey
[5] Micro and Nanotechnology Program of Graduate School of Natural and Applied Sciences, Middle East Technical University, Ankara 06800, Turkey
[6] Department of Metallurgical and Materials Engineering, Middle East Technical University, 06800 Ankara, Turkey

E-mail: bilge.yildiz@metu.edu.tr

CrossMark

Abstract
We experimentally demonstrate that two coupled metal nanostructures (MNSs), a silver nanowire and bipyramid, can produce $\sim$30 times enhanced second harmonic generation compared to the particles alone. We develop a simple theoretical model, presenting the path interference effects in the nonlinear response of coupled MNSs. We show that the reason for such an enhancement can be the occurrence of a Fano resonance due to the coupling of the converter MNS to the long-lived mode of the attached MNS.

Keywords: Fano resonance, second harmonic generation, plasmons, nonlinear optics, enhancement

1. Introduction

Typically, nonlinear optical effects appear at very high intensities; that is, nonlinear optical properties of material surfaces can only be revealed by pulsed lasers. In recent studies [1–3], material surfaces or interfaces decorated with metal nanostructures (MNSs) are suggested to act as non-linear conversion agents, since they enhance the local field amplitudes by several orders of magnitude. This property is expected to enable these efficient nonlinear converters to be utilized in many application areas, such as solar energy, molecular switching, photocatalysis, imaging, etc.

MNSs exhibit absorption resonances at optical frequencies. Such excitations may create hot spots on the surfaces of the MNSs. When a quantum dot (QD) is placed in the vicinity of these hot spots, localized surface plasmons interact strongly with the attached QD. The presence of the QD introduces two absorption paths, both lying in the plasmon spectral width [4], hence making them unresolvable. The two paths operate out of phase—one absorbing, while the second emitting—and result in a dip in the absorption spectrum where an absorption peak should be observed instead. Such transparencies in the plasmonic response are referred to as Fano resonances [5]. These are responsible for increased fluorescence of molecules [6] and increased lifetime of plasmonic oscillations [7], which makes coherent plasmon emission possible [8, 9]. Quantum coherence effects can be used to increase the sensitivity of ultrafast response nano-lasers [10] and can enhance amplification [11, 12].

Plasmon oscillations in MNSs concentrate the incident light to nm dimensions, which yield strong enhancement in the field intensities [9]. The enhancement in the intensity
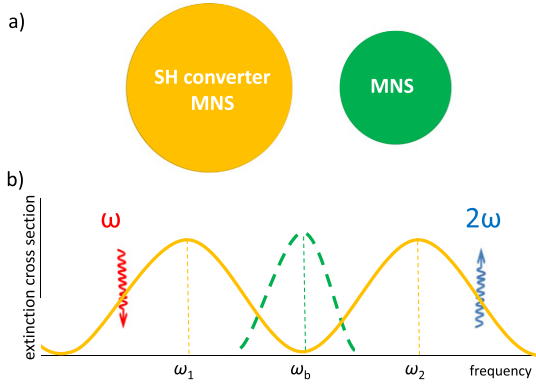
Figure 1. A representative picture of the coupled oscillators and their resonances. The first oscillator (converter) supports two modes, ω_1 and ω_2, where the two frequencies are approximately equal to the driving and SH field frequencies, respectively. The second oscillator is coupled with the first oscillator, introducing path interference effects in the SH response.

leads to the appearance of optical nonlinearities [13] such as as enhanced Raman scattering [14], four-wave mixing [15, 16], two-photon absorption [17–19], and second harmonic generation (SHG) [20–25]. Fano resonances with attached quantum objects can be utilized to enhance [20] and suppress [2] the SHG process in plasmonic particles. The underlying mechanism relies on the cancellation of non-resonant frequency terms, degrading the frequency conversion by hybridized paths [2].

Fano-like resonances can also take place in two coupled classical oscillators [4, 26] without a quantum nature. It is also experimentally demonstrated that coupling with dark modes (which have longer lifetimes) [27–29] can result in Fano resonances.

In this paper, we investigate the second harmonic (SH) signal from coupled silver nanowire (AgNW) and silver bipyramid nanoparticle (AgNP). We observe that the SH signal from the coupled system is highly enhanced compared to MNSs alone. We introduce a very simple theoretical model and show that such a factor of enhancement can be obtained via Fano resonances in the nonlinear response. We show that coupling the converter (AgNW) to the long-lived (10 times), e.g., dark [27], mode of an AgNP can enhance the SH signal in the similar amounts observed in our experiment. Interacting systems of MNSs are experimentally more controllable [4, 21, 26, 28, 29] compared to Fano resonances introduced in coupled plasmon–quantum emitter systems [7, 30]. By the use of carefully designed MNSs, enhanced nonlinear conversion of light can be achieved.

We construct a coupled MNS system composed of an AgNP of ~100 nm size and an AgNW of ~60 nm diameter and several μm length on a dielectric (glass) surface. When a 1064 nm near-infrared (NIR) excitation laser is focused solely on an isolated AgNW, a weak 532 nm SHG signal is generated. Conversely, when the coupled system is excited in the vicinity of the coupling region, the observed SH signal increases up to 30-fold. We have demonstrated this enhancement by performing an *in situ* experiment in which,
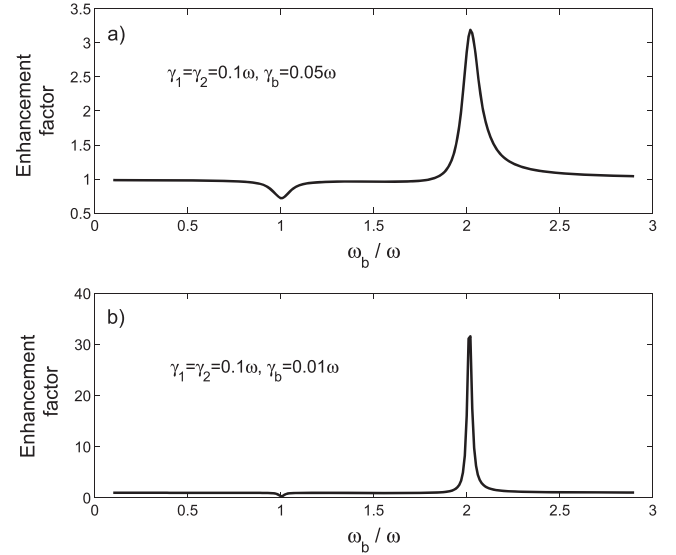

Figure 2. Enhancement factor with changing resonance frequency of the second MNS, ω_b for the coupling of the MNSs with decay rates. (a) $\gamma_1 = \gamma_2 = 0.1\omega$, and $\gamma_b = 0.05\omega$; (b) $\gamma_1 = \gamma_2 = 0.1\omega$, and $\gamma_b = 0.01\omega$. In both cases $\epsilon_p = 0.01\omega$.

as the focus is moved along the AgNW axis, it is found that the generated SH signal increases by a factor of 30 when the focus passes through the AgNP coupled region. The SHG level at the AgNW body a few μm away from the AgNP is at the same level as that of an isolated AgNW. The SH signal from a bare AgNP is found to be only 1/6 of the isolated AgNW. The observed enhancement can be obtained in our model by coupling the converter with an MNS, which has a 10 times longer plasmon lifetime (see figure 2).

2. Theoretical model

In this section, we develop a theoretical model describing the SH response of a system of two coupled plasmonic oscillators. We introduce the effective Hamiltonian for the system and derive the equations of motion for the plasmon polariton (PP) mode fields. We numerically time-evolve the equations to obtain the steady-state occupations of the plasmon modes and show that SH conversion generation can be either enhanced or suppressed by choosing an appropriate MNS supporting a particular frequency mode.

We treat the MNSs as if they do not have a spatial extent; i.e., they are point particles. In the physical situation, however, the particles must have sizes, and, hence, there must be retardation effects. In [2], the coupling of a MNS and a quantum emitter object is treated with the same theoretical model. It is shown that the simple model can well predict the amount and the spectral position of the SHG enhancement by comparing the results with the simulations performed by using MNPBEM Toolbox in MATLAB [31]. The simulations take the retardation effects into account; the physical objects are simulated with their true geometries.

2.1. The model system

We consider two MNSs that support plasmonic excitations at optical wavelengths. The MNSs interact with each other due to induced charge oscillations. The first MNS supports two plasmon modes of resonances ω_1 and ω_2 in the relevant frequency regime (see figure 1(b) solid yellow curve). The shape of the second MNS is chosen so that it has a single plasmonic response peaking at ω_b (see figure 1(b) dashed green curve), near the ω_2 mode of the converter MNS.

The converter MNS has a non-centrosymmetric shape (the spherical shape in figure 1(a) is for demonstrative purposes), which enables the SH process. In the model, we consider only the two plasmon modes in which the converter is driven (ω_1) by the strong laser (ω) and the mode (ω_2), into which the conversion process (2ω) takes place. In general, however, the converter MNS may support many plasmon modes in between ω_1 and ω_2 modes or out of the region covered by the two modes. We neglect the coupling of ω and 2ω excitations to other modes for the sake of obtaining a simple model. We aim for a basic physical picture. The ω_2 mode of the converter is coupled to the ω_b mode of the second MNS. Only for being able to track the leak of the 2ω oscillations from the ω_b mode to other modes in the converter MNS, we also take the coupling of the ω_b with the ω_1 mode into account.

2.2. Hamiltonian

The dynamics of the system is as follows. The incident strong driving field, $\varepsilon_p \mathrm{e}^{-\mathrm{i}\omega t}$, is coupled to the ω_1 mode of the converter and induces plasmon oscillations with frequency ω. The plasmon field ($\hat{a}_1$) produced by the localized surface plasmon excitation yields to a strong electromagnetic field in the plasmonic converter. This localized strong field enables multiphoton (plasmon) processes to come into play. The field oscillating at frequency ω, trapped in the ω_1 plasmon polarization field, gives rise to the SH polarization oscillations at 2ω in the ω_2 mode. Two plasmons in the ω_1 mode combine [32] and generate a 2ω plasmon in the ω_2 mode. It is experimentally demonstrated [33] that the SHG process takes place in plasmonic materials through plasmons. Conversion is carried through such a mechanism, since the overlap integral of the process, $\chi^{(2)} \sim E_1^2(\mathbf{r})E_2^*(\mathbf{r})$, highly increases due to the localization of both plasmon modes [34]. The ω_b mode of the second MNS interacts with both the ω_1 and ω_2 modes. The interaction strengths can be tuned either by varying ω_b or by changing the position or shape of the second MNS (i.e., changing the overlap integral).

The total Hamiltonian can be written as the sum of the energies of the plasmons in the first ($\hat{H}_a$) and the second ($\hat{H}_b$) MNSs, the interaction between the MNSs ($\hat{H}_{int}$), the energy supplied by the incident field ($\hat{H}_p$), and the term governing the SHG process ($\hat{H}_{sh}$),

$$\hat{H} = \hat{H}_a + \hat{H}_b + \hat{H}_{int} + \hat{H}_p + \hat{H}_{sh} \tag{1}$$

where

$$\hat{H}_a = \hbar\omega_1 \hat{a}_1^\dagger \hat{a}_1 + \hbar\omega_2 \hat{a}_2^\dagger \hat{a}_2, \tag{2}$$

$$\hat{H}_b = \hbar\omega_b \hat{b}^\dagger \hat{b}, \tag{3}$$

$$\hat{H}_{int} = \hbar \left(f_1 \hat{a}_1^\dagger \hat{b} + f_1^* \hat{a}_1 \hat{b}^\dagger\right) + \hbar \left(f_2 \hat{a}_2^\dagger \hat{b} + f_2^* \hat{a}_2 \hat{b}^\dagger\right), \tag{4}$$

$$\hat{H}_p = \mathrm{i}\hbar \left(\hat{a}_1^\dagger \epsilon_p \mathrm{e}^{-\mathrm{i}\omega t} - \hat{a}_1 \epsilon_p^* \mathrm{e}^{\mathrm{i}\omega t}\right), \tag{5}$$

$$\hat{H}_{sh} = \hbar\chi^{(2)}(\hat{a}_2^\dagger \hat{a}_1 \hat{a}_1 + \hat{a}_1^\dagger \hat{a}_1^\dagger \hat{a}_2). \tag{6}$$

$\hat{a}_1$ and $\hat{a}_2$ are the annihilation operators for the collective plasmon excitations in the first MNS, corresponding to the modes with resonance frequencies ω_1 and ω_2, respectively. Similarly, $\hat{b}$ is the annihilation operator for the ω_b mode of the second MNS. ($\hat{a}_1$, $\hat{a}_2$, and $\hat{b}$ will represent the amplitudes of the related plasmon oscillations.) f_1 (f_2) is the coupling matrix element between the field induced by the $\hat{a}_1$ ($\hat{a}_2$) mode of the SH converter (first MNS) and the $\hat{b}$ mode of the second MNS. Equation (5) describes the energy contribution of the incident field, which drives the $\hat{a}_1$ PP mode. In equation (6), two low energetic plasmons in the $\hat{a}_1$, mode oscillating at ω, combine to generate a SH plasmon in the $\hat{a}_2$ mode, oscillating at 2ω. The parameter $\chi^{(2)}$, in units of frequency, is proportional to the SH susceptibility of the oscillator.

We use the Heisenberg equation of motion, $\mathrm{i}\hbar\dot{\hat{A}} = [\hat{A}, \hat{H}]$ for any operator $\hat{A}$, to derive the time evolution of the plasmon amplitudes. After obtaining the quantum dynamics of each mode, since we are not interested in the entanglement features but only in intensities, we substitute the quantum operators $\hat{a}_1$, $\hat{a}_2$, and $\hat{b}$ with their expectation values, α_1, α_2, and α_b. We plug in the damping rates for the PP fields, namely γ_1, γ_2, and γ_b, respectively. Consequently we obtain the following equations for the plasmon amplitudes.

$$\dot{\alpha}_1 = (-\mathrm{i}\omega_1 - \gamma_1)\alpha_1 - f_1 \alpha_b + \epsilon_p \mathrm{e}^{-\mathrm{i}\omega t} - 2\mathrm{i}\chi^{(2)}\alpha_1^* \alpha_2 \tag{7}$$

$$\dot{\alpha}_2 = (-\mathrm{i}\omega_2 - \gamma_2)\alpha_2 - f_2 \alpha_b + \mathrm{i}\chi^{(2)}\alpha_1^2 \tag{8}$$

$$\dot{\alpha}_b = (-\mathrm{i}\omega_b - \gamma_b)\alpha_b - f_1 \alpha_1 - \mathrm{i}f_2 \alpha_2. \tag{9}$$

In the steady state, the oscillation modes can only support the driving frequency (ω) and the SH-generated frequency (2ω) of the form

$$\alpha_1 = \alpha_1^{(1)}\mathrm{e}^{-\mathrm{i}\omega t} + \alpha_1^{(2)}\mathrm{e}^{-\mathrm{i}2\omega t}, \tag{10}$$

$$\alpha_2 = \alpha_2^{(1)}\mathrm{e}^{-\mathrm{i}\omega t} + \alpha_2^{(2)}\mathrm{e}^{-\mathrm{i}2\omega t}, \tag{11}$$

$$\alpha_b = \alpha_b^{(1)}\mathrm{e}^{-\mathrm{i}\omega t} + \alpha_b^{(2)}\mathrm{e}^{-\mathrm{i}2\omega t}. \tag{12}$$

Amplitudes $\alpha_1^{(1)}$, $\alpha_2^{(1)}$, and $\alpha_b^{(1)}$ are the amplitudes of linear plasmon oscillations (ω), and $\alpha_1^{(2)}$, $\alpha_2^{(2)}$, and $\alpha_b^{(2)}$ are the amplitudes of the SH (2ω) plasmon oscillations.

We numerically time-evolve equations (7)–(9) and then obtain the time behaviour after the steady state has been reached. Using the Fourier transform technique we determine the steady-state amplitudes, $\alpha_1^{(2)}$, $\alpha_2^{(2)}$, and $\alpha_b^{(2)}$, the amplitudes of the SH oscillations. The number of the SH plasmons can be determined by summing over the plasmons generated in all

three modes as

$$N_{sh} \equiv \left| \alpha_1^{(2)} \right|^2 + \left| \alpha_2^{(2)} \right|^2 + \left| \alpha_b^{(2)} \right|^2. \qquad (13)$$

We note that $e^{-i2\omega t}$ oscillations in the α_1 and α_b modes are not generated in these modes. They are, rather, transferred from the α_2 mode due to interactions.

2.3. Tuning the second harmonic conversion

We are interested in the enhancement and suppression of the SHG from the first MNS, in the presence of alternative absorption/emission pats, due to the coupling with the second MNS. We compare the number of 2ω plasmons generated in the presence of coupling ($f_1 \neq 0, f_2 \neq 0$), N_{sh}, to the number of 2ω plasmons in the absence of coupling ($f_1 = 0, f_2 = 0$), $N_{sh}^{(0)}$. Thus, we define the enhancement factor as the ratio of N_{sh} to $N_{sh}^{(0)}$.

$$\text{Enhancement factor} \equiv \frac{N_{sh}}{N_{sh}^{(0)}} \qquad (14)$$

In order to identify the spectral positions of the nonlinear Fano resonances, we calculate the SHG enhancement factor for different resonance frequencies, ω_b, of the second MNS. In our simulations, we fix the parameters $\omega_1 = \omega$, $\omega_2 = 2\omega$, $\gamma_1 = \gamma_2 = 0.1\omega$, $f_1 = 0.2\omega$, and $f_1 = 0.8\omega$. In figures 2(a) and (b), we set the decay rate of the second MNS as $\gamma_b = 0.05\omega$ and $\gamma_b = 0.01\omega$, respectively.

Figure 2(a), where $\gamma_b = 0.05\omega$, shows that in the case of two coupled MNSs, the SHG can be enhanced more than three times as compared to the case of the first MNS alone. Maximum enhancement is obtained when the resonance of the second MNS is tuned to $\omega_b = 2.02\omega$. Conversely the SHG can be suppressed to 0.72 when ω_b is tuned to $\omega_b = 1\omega$. Figure 2(b) shows that when a second MNS with smaller damping ($\gamma_b = 0.01\omega$) is used, a smaller suppression but much larger 2(a) enhancement can be obtained. At $\omega_b = 2.02\omega$ ($\omega_b = 1\omega$), the enhancement (suppression) factor of 32 (0.31) is found.

The emergence of enhancement at about $\omega_b \approx 2\omega$ can be understood using the arguments given in [2]. The off-frequency term, that is, $\omega_2 - 2\omega$, is cancelled by an auxiliary term that emerges due to the path interference effects (see the discussion below equation (9) in [2]). Suppression at $\omega_b = 1\omega$ takes place, since the linear path interference does not allow the excitation at the driving frequency ω. When the linear response is suppressed, smaller ω ($\hat{a}_1$) plasmon intensities result in less SH conversion.

In the following section, we report the results of an experiment on an AgNW–AgNP system locally illuminated with a Gaussian beam source.

3. Experiment

In this section we explain the details of the experimental study on a similar system to the one studied within the theoretical
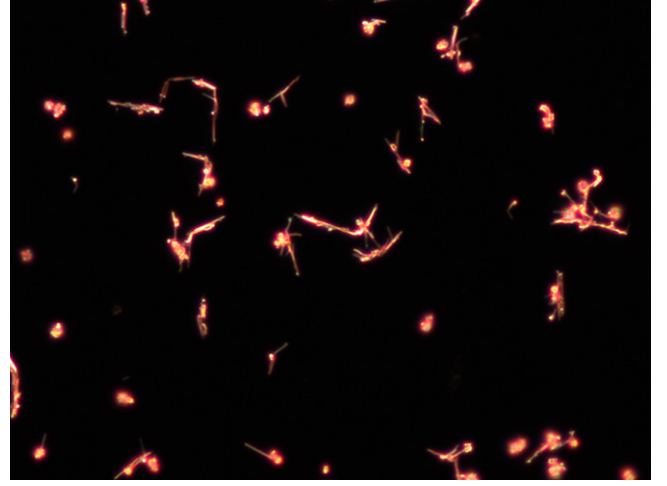

Figure 3. A darkfield image of the AgNW–AgNP network deposited on microscope cover-slip. Light-colored, long straight features in the image represent the AgNWs, and the bright intense spots represent the AgNPs.

model, a system of two coupled plasmonic oscillators; a silver nanowire and a silver nanoparticle.

3.1. Colloidal solution preparation procedure

Silver nanowires are synthesized by a self-seeding polyol process. In this technique, an inorganic salt is reduced by a polyol, and an agglomeration of particles is prevented by the addition of a surfactant, which is commonly called poly-vinylpyrrolidone (PVP). The required chemicals were bought from Sigma-Aldrich. 7 mg of NaCl is added into 10 mL of 0.45 M ethylene glycol (EG) solution of PVP and heated at 170 °C. By using an injection pump, a solution of 0.12 M AgNO$_3$ in 5 mL of EG is added drop-wise at a rate of 5 mL h^{-1}. During this process, the solution is stirred at a 1000 rpm rate by a magnetic stirrer. After the drop-wise EG addition process, the solution is heated up at 170 °C for 30 min and is cooled to room temperature. To enable the removal of the polymer from the solution, the diluted solution with acetone is centrifuged two times for 20 min at 6000 rpm. Afterwards, wires are dispersed in ethanol and centrifuged again under the same conditions. At the end of this procedure, nanowires with 60 nm diameter and a length of 8–10 μm are obtained.

A solution containing bipyramids of metallic silver is synthesized with the polymer-mediated polyol process as well. 94 mM AgNO$_3$ is added to 3 mL EG solution. Another 3 mL of EG solution containing 0.11 mM NaBr and 144 mM PVP is prepared, and the two solutions are added dropwise into a heated EG solution of 5 mL in an oil bath at 160 °C, which contains 30 μL of 10 mM NaBr. After 5 h, the bipyramid solution with an average size of 150 nm is obtained [35, 36]. The synthesis procedure leaves the AgNWs and AgNPs with a polymer coating of about 3–4 nm thickness.

The resulting AgNPs are co-deposited on the same substrates of AgNWs to obtain a network of NW–NP complexes, which are ultimately asymmetric structures and cover a
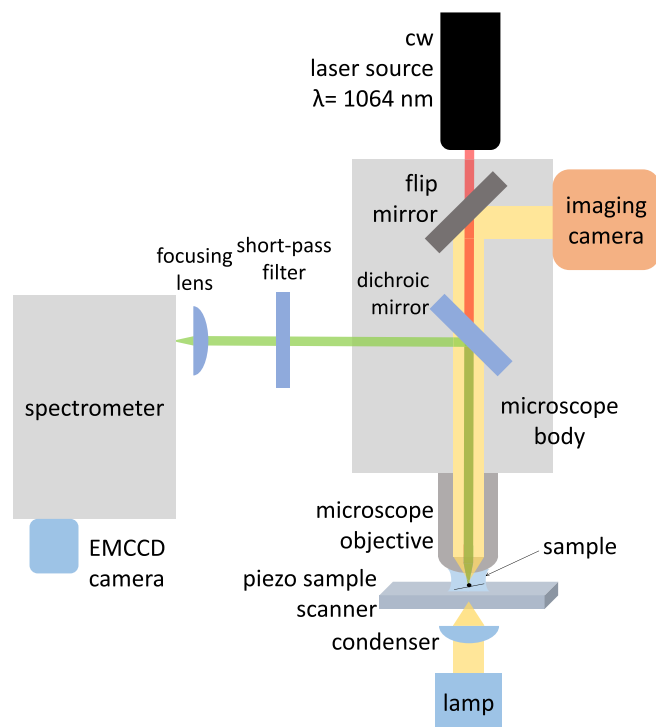
Figure 4. The experimental setup is composed of a cw Nd:YAG laser with $\lambda = 1064$ nm, a long-pass dichroic mirror, a flip mirror, a microscope with objective, a piezo sample scanner, a short-pass filter (cut off at 800 nm), a focusing lens, a spectrometer with an EMCCD camera, an illumination lamp, a condenser, and an imaging camera.

macroscopically large area. Such coated surfaces are first imaged by darfield microscopy to ensure the existence of the complexes (figure 3). The AgNPs are observed to display different colors, such as green and blue, under white-light illumination as a result of their size-dependent plasmon resonance in the visible range. The AgNWs are observed to show a reddish glimmer as a result of a shift of their plasmon resonance towards NIR due to the high-aspect ratio of their geometry. A combination of two such Ag nanostructures is what we expect to boost the SHG due to conversion of NIR plasmons to visible plasmons upon interaction of the NWs with the NPs .

3.2. Optical measurements

In figure 5 we show that the AgNWs do possess a manifold of plasmon resonances comparable to the sketched model in figure 1. The data shows differential absorption (figure 5(b)) which is calculated from the original absorption spectrum measurement (figure 5(a)) performed on a liquid dispersion of AgNWs at 0.125 mg ml^{-1} concentration. The dominant plasmon resonance [37, 38] centered at 390 nm (769 THz) is subtracted from the measured data by performing a peak fit. The residual differential absorption curve (in black) is displayed in THz units to allow for direct comparison to figure 1. In figure 5 we also show three Gaussian peaks, two of which are much like the ω_1, ω_2 (orange solid) plasmon bands in the model.
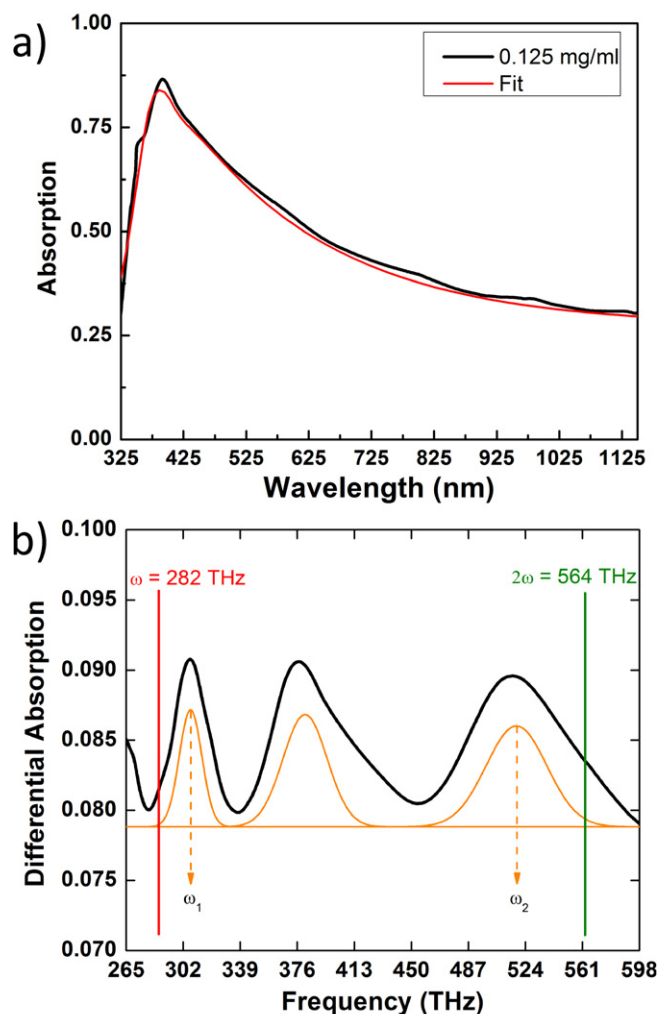

Figure 5. (a) The absorption spectrum of liquid dispersion of AgNW (black) and a peak fit to the strongest plasmon mode at 390 nm (red); (b) The differential absorption curve after the contribution of the strong plasmon peak is subtracted (black), the two Gaussian peaks representing the ω_1, ω_2 (orange solid) plasmon bands.

We used an inverted microscope (Zeiss model Axiovert 200) with a 63X (1.4 NA) objective lens for our experiments. In figure 4, a scheme of the experimental setup is displayed. We used a cw Nd:YAG laser (Cobolt model Rumba) with wavelength of $\lambda = 1064$ nm and 500 mW output power as the excitation source. The NIR signal was delivered from the back port of the microscope, resulting in an intensity of 40 MW cm^{-2} on the sample. The resulting SHG from the AgNW–AgNP cluster was registered by a spectrometer (Andor models Shamrock 750 spectrograph + Newton 971 electron-multiplied charge coupled device (EMCCD)) in cooperation with a long-pass dichroic mirror cutting off the backscattered 1064 nm signal and reflecting a band of 520–750 nm.

We first record a transmission image by the visual inspection camera that works in the visible (see figure 6). The dark figures in the image indicate the location of AgNWs, AgNPs, and their clusters with a very poor resolution. Nevertheless this image is sufficient to locate a candidate
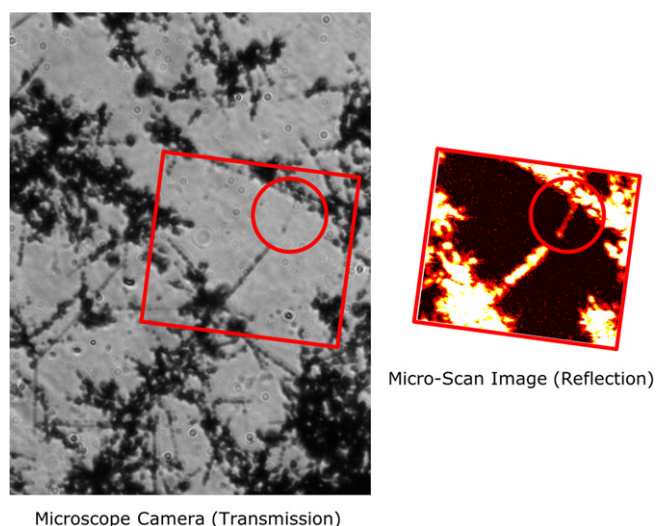
Microscope Camera (Transmission)

Micro-Scan Image (Reflection)

Figure 6. A transmission image by the microscope camera on the left and a micro-scan reflection image of the area, as indicated by the red rectangle, on the right. The red circles show a region with a single AgNW with a single AgNP attached close to its end.
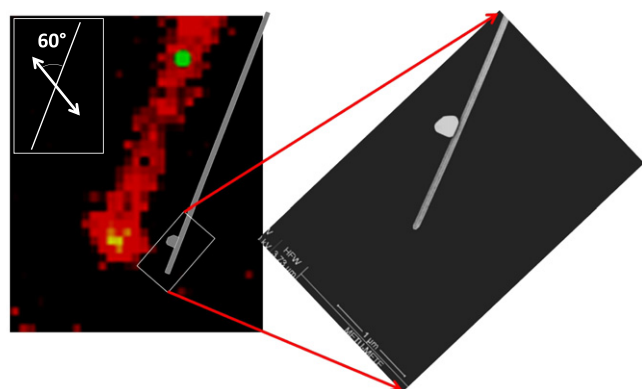

Figure 7. A zoom-in into the encircled region in the micro-scan image along with a sketch of the AgNW–AgNP complex. The SEM image on the right shows the end of the AgNW with high magnification.

Figure 8. (a) The SHG spectra obtained at different positions along the body of the AgNW (inset). The integrated SHG intensity (left vertical axis) and the enhancement factor (right vertical axis) as a function of position on the AgNW. The breadth of the SHG signal peak along the AgNW axis is due to the 1 μm focal spot size. (b) The SHG integral signal intensity as a color bar, and the AgNW along with it, clearly show that the enhancement originates from coupling of the AgNW with the AgNP. The color bar is superposed onto the representative sketch of the system on the right.

region that bears a single AgNW–AgNP complex for further detailed study. The red circle on the transmission image on the left points out a region of possible interest with one NW and NP complex. The red rectangle indicates the region, which is scanned at a high resolution by the piezo-stage. The reflection image produced by the scanning of the same region is given on the right using a 1064 nm NIR laser. The reflection image produced at the illumination wavelength shows intense reflection from crowded clusters as well as a single straight feature, which is the isolated part of a single AgNW and an AgNP attached towards the end of the AgNW. The faint straight shadow on the left image and a dark spot at its end appear as a straight bright feature on the left with a brighter spot at its end that indicates the attached AgNP.

Such AgNW–AgNP complexes are often encountered upon inspection of these samples with a scanning electron microscope (SEM). Figure 7 shows a zoomed version of the encircled straight part of the micro-scan image along with a
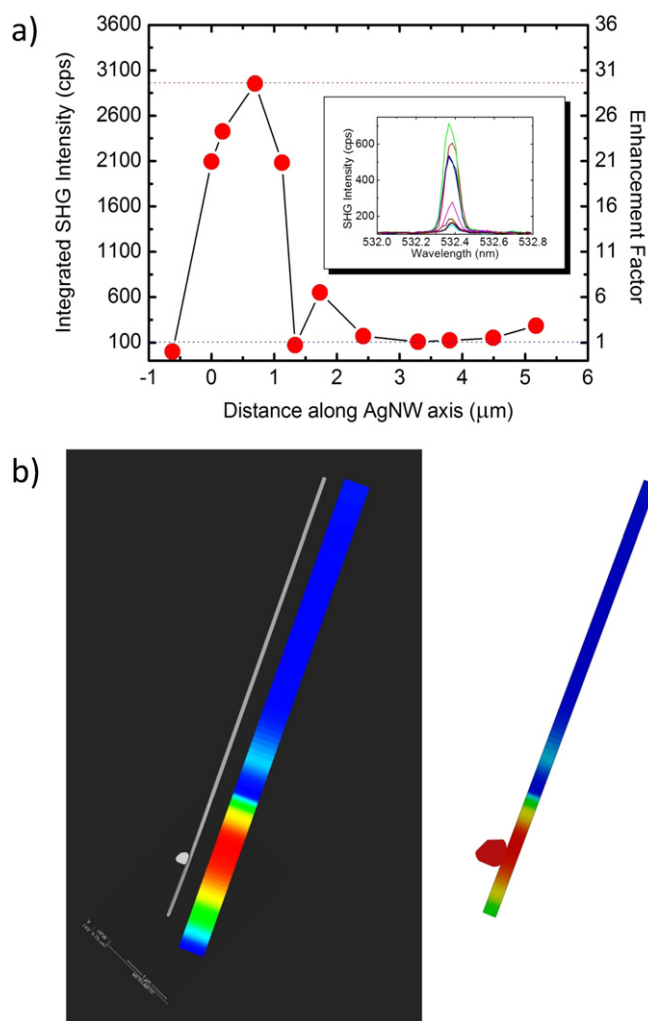
representative sketch of the AgNW–AgNP complex drawn to scale. An SEM image is provided on the right that shows a highly magnified image of the end of the AgNW with the attached AgNP along its body. The AgNW is typically 50–60 nm in diameter and can be as long as 5–10 μm. The AgNPs are typically of 50–150 nm size.

3.3. Experimental results

By the help of the micro-scan image, we can direct our focal spot at any pixel of choice and acquire SHG spectra using a spectrometer/EMCCD combination. While moving the diffraction-imited illumination spot stepwise along the axis of the AgNW, an SHG spectrum is acquired at each step, and the acquired spectra are plotted (figure 8(a), inset). These spectra are acquired for 60 s and integrated over the SHG band. The

integral SHG signal is plotted against the distance along the AgNW axis (figure 8(a)). The excitation polarization is linear and is in the plane of the sample surface. The white arrow in the left inset in figure 7 shows the polarization direction, which is 60° to this particular AgNW that we studied.

There are three major results that we obtain. (i) When the illumination spot is not located on the AgNW, no SHG signal is registered, so the SHG originates genuinely from the plasmonic structure. (ii) We observe the SHG even with cw illumination (50 mW on the sample) from AgNW plasmonic structures. (iii) The SHG signal is enhanced by a factor of about 30 when the illumination spot is on the AgNP–AgNW complex with respect to the body of the AgNW alone.

A better visual represantation of the SHG intensity distribution as a function of position along the AgNW axis is given in figure 8(b). A color bar is produced from the integral SHG signal and displayed in parallel with the actual SEM image and its representative straight extension. The SHG signal clearly appears, starting from the end of the AgNW, and reaches its maximum around where the AgNP is attached to the AgNW. An overlap of the color bar with a representation of such an AgNW–AgNP plasmonic hybrid complex on the right clearly depicts the observed effect: An enhanced SH conversion spot is constructed by the hybridization of the AgNW and AgNP plasmons.

4. Discussion and conclusions

In this paper we study the tunability of SHG from a coupled system of a metal nano particle and a nanowire. Our experiments show that the SHG from nanoparticles or nanowires can be enhanced about 30 times as compared to the uncoupled ones because of path interference effects. We also introduce a single theoretical model and demonstrate the origin of the enhancement in our experiment.

AgNP and NW samples are illuminated with continuous-wave NIR laser source of 1064 nm wavelength at different focal points with a focal spot size 1 μm diameter. First, AgNW and AgNP samples of typical sizes 5 μm and 100 nm, respectively, are illuminated separately, and the SH response is recorded. Second, the two MNSs are combined, and a representative coupled MNS is identified. The focus of the NIR laser is moved stepwise along the axis, and the SH response at 532 nm wavelength is recorded at each step (figure 8). It is observed that when the laser focus is in the region containing the coupled AgNP, the SH signal is enhanced up to 30 times as compared to the AgNP-free regions on the AgNW axis.

Our experimental results can be interpreted by the help of the developed theoretical model examining the effects of coupling of an MNS with an SH converter MNS. We show that the enhancement factor (∼30) observed in the experiment can be obtained by attaching a higher-quality MNS to the SH converter MNS. The attached MNS has a distorted bipyramidal shape and can support dark modes [27] with relatively longer lifetimes than that of bright modes. Therefore in our experiment AgNW plays the role of SH converter, and

bipyramid AgNP is the coupled higher-quality plasmonic oscillator. This is also confirmed by control experiments performed on AgNW and AgNP samples separately, where the former is found to generate ∼6 times higher SH conversion. It can be noted that the AgNP size effect is incorporated to our model through the f_1 and f_2 parameters in equation (4). AgNPs with different sizes are expected to have different ω_b positions, which result in different levels of overlaps between ω_1 and ω_2, and, hence, different magnitudes of f_1 and f_2, respectively. The magnitudes of these parameters play an important role in the SHG enhancement.

Alzar *et al* show that absorption cancellations due to Fano resonances can be achieved in entirely classical systems [4], which are observed in our and recent experiments [1, 16, 20–22]. We approach the problem with a simple model of two coupled oscillators that have different damping rates. We reveal the enhancement/suppression effects on the spectrum of the nonlinear conversion using simple arguments.

References

[1] Luk'yanchuk B, Zheludev N I, Maier S A, Halas N J, Nordlander P, Giessen H and Chong C T 2010 The Fano resonance in plasmonic nanostructures and metamaterials *Nat. Mater.* **9** 707–15
[2] Turkpence D, Tasgin M E, Akguc G B and Bek A 2014 Engineering nonlinear response of nanomaterials using Fano resonances *J. Opt.* **16** 105009
[3] Salakhutdinov I, Kendziora D, Abak M K, Turkpence D, Piantanida L, Fruk L, Tasgin M E, Lazzarino M and Bek A 2014 Plasmonic non-linear conversion of continuous wave light by gold nanoparticle clusters with fluorescent protein loaded gaps (arXiv:1402.5244)
[4] Alzar C L G, Martinez M A G and Nussenzveig P 2002 Classical analog of electromagnetically induced transparency *Am. J. Phys.* **1** 37
[5] Miroshnichenko A E, Kivshar Y S and Flach S 2010 Fano resonances in nanoscale structures *Rev. Mod. Phys.* **82** 2257–98
[6] Ayala-Orozco C, Liu J G, Knight M W, Wang Y, Day J K, Nordlander P and Halas N J 2014 Fluorescence enhancement of molecules inside a gold nanomatryoshka *Nano Lett.* **14** 2926–33
[7] Tasgin M E 2013 Metal nanoparticle plasmons operating within a quantum lifetime *Nanoscale* **5** 8616–24
[8] Noginov M A, Zhu G, Belgrave A M, Stout S, Bakker R, Shalaev V M, Narimanov E E, Herz E, Suteewong T and Wiesner U 2009 Demonstration of a spaser-based nanolaser *Nature* **460** 1110–12

[9] Stockman M I 2011 Nanoplasmonics: past, present, and glimpse into future *Opt. Express* **19** 22029–106

[10] Voronine D V, Huo W and Scully M 2014 Ultrafast dynamics of surface plasmon nanolasers with quantum coherence and external plasmonic feedback *J. Opt.* **16** 114013

[11] Dorfman K E, Jha P K, Voronine D V, Genevet P, Capasso F and Scully M O 2013 Quantum coherence enhanced surface plasmon amplification by stimulated emission of radiation *Phys. Rev. Lett.* **111** 043601

[12] Voronine D V, Sinyukov A M, Hua X, Munusamy E, Ariunbold G, Sokolov A V and Scully M O 2015 Complex line shapes in surface enhanced coherent Raman spectroscopy *J. Mod. Opt.* **62** 90–96

[13] Kauranen M and Zayats A V 2012 Nonlinear plasmonics *Nat. Photonics* **6** 737–48

[14] Sharma B, Frontiera R R, Henry A-I, Ringe E and van Duyne R P 2012 Sers: materials, applications, and the future *Mater. Today* **15** 16

[15] Genevet P, Tetienne J P, Blanchard M A, Kats R, Capasso F, Gatzogiannis E and Scully M O 2010 Large enhancement of nonlinear optical phenomena by plasmonic nanocavity gratings *Nano Lett.* **10** 4880–83

[16] Renger J, Quidant R and Novotny L 2011 Enhanced nonlinear response from metal surfaces *Opt. Express* **19** 1777–85

[17] Cox J D, Singh M R, von Bilderling C and Bragas A V 2013 A nonlinear switching mechanism in quantum dot and metallic nanoparticle hybrid systems *Adv. Opt. Mater.* **1** 460–7

[18] Cox J D, Singh M R, Anton M A and Carreno F 2013 Plasmonic control of nonlinear two-photon absorption in graphene nanocomposites *J. Phys.: Condens. Matter* **25** 385302

[19] Racknor C, Singh M R, Zhang Y, Birch D J S and Chen Y 2014 Energy transfer between a biological labelling dye and gold nanorods *Methods Appl. Fluorescence* **2** 015002

[20] Thyagarajan K, Butet J and Martin O J F 2013 Augmenting second harmonic generation using Fano resonances in plasmonic systems *Nano Lett.* **13** 1847–51

[21] Berthelot J, Song M, Rai P, Des Francs G C, Dereux A, Bouhelier A and Bachelier G 2012 Silencing and enhancement of second-harmonic generation in optical gap antennas *Opt. Express* **20** 10498–508

[22] Wunderlich S and Peschel U 2013 Plasmonic enhancement of second harmonic generation on metal coated nanoparticles *Opt. Express* **21** 18611–23

[23] Gao S, Ueno K and Misawa H 2011 Plasmonic antenna effects on photochemical reactions *Acc. Chem Res.* **44** 251–60

[24] Singh M R 2013 Enhancement of the second-harmonic generation in a quantum dot-metallic nanoparticle hybrid system *Nanotechnology* **24** 125701–06

[25] Walsh G F and Dal Negro L 2013 Enhanced second harmonic generation by photonic-plasmonic Fano-type coupling in nanoplasmonic arrays *Nano Lett.* **13** 3111

[26] Tassin P, Zhang L, Zhao R, Jain A, Koschny T and Soukoulis C M 2012 Electromagnetically induced transparency and absorption in metamaterials: the radiating two-oscillator model and its experimental confirmation *Phys. Rev. Lett.* **109** 187401

[27] Panaro S, Nazir A, Liberale C, Das G, Wang H, de Angelis F, Proietti Zaccaria R, di Fabrizio E and Toma A 2014 Dark to bright mode conversion on dipolar nanoantennas: a symmetry-breaking approach *ACS Photonics* **1** 310–14

[28] Artar A, Yanik A A and Altug H 2011 Multispectral plasmon induced transparency in coupled meta-atoms *Nano Lett.* **11** 1685–9

[29] Cetin A E, Artar A, Turkmen M, Yanik A A and Altug H 2011 Plasmon induced transparency in cascaded p-shaped metamaterials *Opt. Express* **19** 22607–18

[30] Clark H A, Campagnola P J, Wuskell J P, Lewis A and Loew L M 2000 Second harmonic generation properties of fluorescent polymer-encapsulated gold nanoparticles *J. Am. Chem. Soc.* **122** 10234–35

[31] Hohenester U and Trugler A 2012 MNPBEM–A MATLAB toolbox for the simulation of plasmonic nanoparticles *Comput. Phys. Commun.* **183** 370–81

[32] Finazzi M and Ciccacci F 2012 Plasmon-photon interaction in metal nanoparticles: second-quantization perturbative approach *Phys. Rev.* B **86** 035428

[33] Grosse N B, Heckmann J and Woggon U 2012 Nonlinear plasmon-photon interaction resolved by k-space spectroscopy *Phys. Rev. Lett.* **108** 136802

[34] Ginzburg P, Krasavin A, Sonnefraud Y, Murphy A, Pollard R J, Maier S A and Zayats A V 2012 Nonlinearly coupled localized plasmon resonances: resonant second-harmonic generation *Phys. Rev.* B **86** 085422

[35] Coskun S, Aksoy B and Unalan H E 2011 Polyol synthesis of silver nanowires: an extensive parametric study *Cryst. Growth Des.* **11** 4963–9

[36] Wiley B J, Xiong Y, Xia Y, Li Z Y and Yin Y 2006 Right bipyramids of silver: a new shape derived from single twinned seeds *Nano Lett.* **6** 765–8

[37] Kottmann J P, Martin O J, Smith D R and Schultz S 2001 Plasmon resonances of silver nanowires with a nonregular cross section *Phys. Rev.* B **64** 235402

[38] Zhu J-J, Kan C-X, Wan J-G, Han M and Wang G-H 2011 High-yield synthesis of uniform Ag nanowires with high aspect ratios by introducing the long-chain PVP in an improved polyol process *J. Nanomater.* **2011** 40